

How large is the Knudsen number reached in fluid dynamical simulations of ultrarelativistic heavy ion collisions?

H. Niemi^{a,b} and G. S. Denicol^c

^a*Department of Physics, University of Jyväskylä,*

P.O. Box 35 (YFL), FI-40014 University of Jyväskylä, Finland

^b*Helsinki Institute of Physics, P.O.Box 64, FI-00014 University of Helsinki, Finland and*

^c*Department of Physics, McGill University, 3600 University Street, Montreal, Quebec, H3A 2T8, Canada*

We investigate the applicability of fluid dynamics in ultrarelativistic heavy ion (AA) collisions and high multiplicity proton nucleus (pA) collisions. In order for fluid dynamics to be applicable the microscopic and macroscopic distance/time scales of the system have to be sufficiently separated. The degree of separation is quantified by the ratio between these scales, usually referred to as the Knudsen number. In this work, we calculate the Knudsen numbers reached in fluid dynamical simulations of AA and pA collisions at RHIC and LHC energies. For this purpose, we consider different choices of shear viscosity parametrizations, initial states and initialization times. We then estimate the values of shear viscosity for which the fluid dynamical description of ultrarelativistic AA and pA collisions breaks down. In particular, we study how such values depend on the centrality, in the case of AA collision, and multiplicity, in the case of pA collision. We found that the maximum viscosity in AA collisions is of the order $\eta/s \sim 0.1 \dots 0.2$, which is similar in magnitude to the viscosities currently employed in simulations of heavy ion collisions. For pA collisions, we found that such limit is significantly lower, being less than $\eta/s = 0.08$.

I. INTRODUCTION

The main goal of the experimental heavy ion collision program at RHIC and LHC is to verify the existence of a nearly thermal quark-gluon plasma (QGP), as well as to determine its properties. Currently, the several collaborations participating in these experiments are able to provide a wealth of experimental data on the transverse momentum of hadrons, leptons and photons produced in the collisions. However, interpreting such findings and extracting the properties of the QGP from them is a complicated task, requiring a good theoretical understanding of the dynamics of the system produced in the reaction.

Relativistic fluid dynamics is currently the main theoretical tool used to describe the spacetime evolution of the bulk matter formed in ultrarelativistic heavy ion collisions. Such approach has been particularly successful in predicting and understanding the azimuthal asymmetries of the transverse momentum spectra of charged hadrons [1, 2]. In this approach, such azimuthal asymmetries emerge from a fluid-dynamical response to the azimuthally inhomogeneous initial geometry of the matter produced. Currently, there are several studies indicating that the effective shear viscosity to entropy density ratio η/s required to describe the data must be small, of the order of $\eta/s \sim 0.1 \dots 0.2$ [3–14].

On the other hand, such collisions occur under extreme conditions that may even question the validity of a fluid-dynamical description. The system is created in a very small volume and lives for a very short time, rendering the applicability of fluid dynamics questionable. Recently, the situation was made more extreme by the inclusion of event by event fluctuations in the initial state of the system [15, 16], which serve to increase the size of its energy density and flow velocity gradients. While in previous fluid-dynamical models such gradients

were of the order of the system size (~ 10 fm), now the fluctuations are thought to be sub-fermionic [17, 18]. If fluid dynamics is in fact able to describe the time evolution of energy density fluctuations on such small distance scales, it may be even applicable to model the dynamics of proton-nucleus collisions [19–21].

For this reason, it is important to study the domain of validity of fluid dynamics in ultrarelativistic heavy ion collisions. The applicability of fluid dynamics is traditionally quantified in terms of the Knudsen number, a ratio between the microscopic and macroscopic length scales involved in the problem. A small Knudsen number implies a wide separation between the microscopic and macroscopic distance/time scales making it possible for the system to approach local thermodynamic equilibrium in macroscopic volumes. A large Knudsen number usually results in a strong deviation from local thermodynamic equilibrium, rendering the applicability of fluid dynamics doubtful. So far, a detailed study of the values of Knudsen numbers that may be reached in the realistic fluid-dynamical modeling of heavy ion collisions has not been performed.

In this work, we estimate the magnitude of the (local) Knudsen numbers that can be reached in the fluid-evolution of the quark-gluon plasma formed in heavy ion (AA) collisions, and in proton-nucleus (pA) collisions. We consider several choices of gradients to quantify the macroscopic length/time scales: 1) the expansion rate, 2) energy density gradient, 3) the shear tensor, 4) the vorticity tensor, and 5) the proper time derivative of the flow velocity. We then investigate the applicability of fluid dynamics in AA and pA collisions at RHIC and LHC energies. Here, we do not consider fluctuations in the initial energy density profiles. Rather, we study how the applicability of fluid dynamics depends on the scale of density and velocity fluctuations by varying the sys-

tem size. This is done so by considering several centrality classes, for the case of AA collisions, and several multiplicities for pA collisions. We then study the magnitude of the viscosity that the fluid-dynamical modeling can handle before it breaks down.

This paper is organized as follows. In Sec. II we shortly introduce the theory of transient fluid dynamics, and in Sec. III we discuss the conditions for which this theory is applicable. The details of the fluid dynamical modeling of AA and pA collisions are specified in Sec. IV. In Sec. V we show the main results of this paper. Finally, in Sec. VI we discuss the implications of our results and make our concluding remarks.

We use natural units $\hbar = c = k_B = 1$, and the sign convention of the metric tensor is $g_{\mu\nu} = \text{diag}(+, -, -, -)$.

II. RELATIVISTIC FLUID DYNAMICS

Fluid dynamics is an effective theory that describes the long distance, long time limit of an underlying microscopic theory [22]. In this case the state of the fluid can be characterized solely by the densities and currents associated to conserved quantities, such as the energy-momentum tensor, $T^{\mu\nu}$, and net charge 4-currents, N^μ (e.g. the baryon number 4-current in heavy ion collisions.) The dynamical evolution of $T^{\mu\nu}$ and N^μ is given by the continuity equations,

$$\partial_\mu T^{\mu\nu} = 0, \quad \partial_\mu N^\mu = 0, \quad (1)$$

which are completely general and follow solely from the fact that energy, momentum, and charge are conserved on a microscopic level.

The energy-momentum tensor and charge 4-current can be tensor decomposed in terms of the fluid 4-velocity, u^μ ,

$$T^{\mu\nu} = \varepsilon_0 u^\mu u^\nu - \Delta^{\mu\nu} (P_0 + \Pi) + \pi^{\mu\nu}, \quad (2)$$

$$N^\mu = n_0 u^\mu + q^\mu, \quad (3)$$

where ε_0 is the energy density, P_0 the thermodynamic pressure, n_0 the net-charge density, Π the bulk viscous pressure, q^μ the net-charge diffusion 4-current, and $\pi^{\mu\nu}$ the shear-stress tensor. For the sake of convenience, we further introduced the projection operator onto the 3-space orthogonal to the velocity, $\Delta^{\mu\nu} = g^{\mu\nu} - u^\mu u^\nu$. It is also convenient to define a double projection operator, that is symmetric and traceless, $\Delta_{\alpha\beta}^{\mu\nu} = (\Delta_\alpha^\mu \Delta_\beta^\nu + \Delta_\beta^\mu \Delta_\alpha^\nu)/2 - \Delta^{\mu\nu} \Delta_{\alpha\beta}/3$.

Since the conservation laws lead to only 5 equations of motion and conserved currents, $T^{\mu\nu}$ and N^μ , contain 14 degrees of freedom, the system of equations is not yet closed and one still needs to provide 9 additional equations of motion. These would correspond to the time evolution equations for the dissipative currents, Π , q^μ , and $\pi^{\mu\nu}$.

In heavy ion collisions, one must model the evolution of the matter using a relativistic formulation of

fluid-dynamics. Traditional formulations, such as Navier-Stokes theory or the gradient expansion [23, 24], do not work since their acausal nature [25] leads to intrinsic instabilities that render the theory useless for practical purposes [26, 27]. This problem is usually solved by employing causal formulations of fluid dynamics, in which the dissipative currents become independent dynamical variables that satisfy relaxation-type equations [28, 29].

There are several formulations of causal fluid dynamics. In this work, we employ the equations derived from kinetic theory in Refs. [28, 30–36]. Such equations include all the possible nonlinear terms that can appear in the time evolution equations for the dissipative currents and in principle increase the domain of applicability. For the purposes of this work, we shall neglect the effects of bulk viscous pressure and net baryon number diffusion, i.e., $\Pi = 0 = q^\mu$. Thus, all dissipative effects originate only from the dynamics of the shear-stress tensor.

The equation of motion for the shear-stress tensor derived from kinetic theory is [31]

$$\begin{aligned} \tau_\pi \dot{\pi}^{\langle\mu\nu\rangle} + \pi^{\mu\nu} &= 2\eta\sigma^{\mu\nu} + 2\tau_\pi \pi_\lambda^{\langle\mu} \omega^{\nu\rangle\lambda} - \delta_{\pi\pi} \pi^{\mu\nu} \theta \\ &- \tau_{\pi\pi} \pi^{\lambda\langle\mu} \sigma_\lambda^{\nu\rangle} + \varphi_7 \pi^{\lambda\langle\mu} \pi_\lambda^{\nu\rangle}. \end{aligned} \quad (4)$$

Above we introduced the shear viscosity, η , shear relaxation time, τ_π , and the remaining transport coefficients of the nonlinear terms $\delta_{\pi\pi}$, $\tau_{\pi\pi}$, and φ_7 . The notation for the transport coefficients was taken from Ref. [31]. We further introduced the shear tensor, $\sigma^{\mu\nu} = \nabla^{\langle\mu} u^{\nu\rangle}$, the expansion rate, $\theta = \nabla_\mu u^\mu$, and the vorticity tensor, $\omega^{\mu\nu} = (\nabla^\mu u^\nu - \nabla^\nu u^\mu)/2$, and used the notation, $\dot{A} \equiv u^\mu \partial_\mu A$, $\nabla^\mu \equiv \Delta^{\mu\nu} \partial_\nu$, and $A^{\langle\mu\nu\rangle} = \Delta_{\alpha\beta}^{\mu\nu} A^{\alpha\beta}$.

In the 14-moment approximation and massless limit, it is possible to show that [31, 33]

$$\tau_\pi = 5 \frac{\eta}{\varepsilon_0 + P_0}, \quad (5)$$

$$\delta_{\pi\pi} = \frac{4}{3} \tau_\pi, \quad (6)$$

$$\tau_{\pi\pi} = \frac{10}{7} \tau_\pi, \quad (7)$$

$$\varphi_7 = \frac{9}{70} P_0^{-1}. \quad (8)$$

In this work, we assume that the above expressions remain valid even for a strongly interacting system, and use them in our simulations. In heavy ion collisions, it is common to assume an effective shear viscosity that is proportional to the entropy density, $\eta_{\text{eff}} = a \times s$, where s is the entropy density and a is a proportionality coefficient. The coefficient a is usually extracted phenomenologically from heavy ion collision experiments and may range from $a = 0, \dots, 0.2$. In this work, we shall consider this effective viscosity, but also use temperature dependent parametrizations of η/s .

III. KNUDSEN NUMBER AND VALIDITY OF FLUID DYNAMICS

As already mentioned, the validity of the fluid-dynamical description can be quantified by the Knudsen number, $\text{Kn} = \ell_{\text{micro}}/L_{\text{macro}}$, where ℓ_{micro} and L_{macro} are the microscopic and macroscopic distance/time scales, respectively. For a dilute gas, ℓ_{micro} is the mean free-path of the particles and one can show that $\tau_{\pi} \sim \ell_{\text{micro}}$. For a strongly interacting system, the microscopic scale is not well known, but we shall continue to assume that it is proportional to the shear relaxation time, that is,

$$\ell_{\text{micro}} \sim \tau_{\pi} = 5 \frac{\eta}{\varepsilon_0 + P_0}. \quad (9)$$

We also note that the shear relaxation time is the only microscopic scale that directly enters into Eq. (4). The macroscopic scale should be estimated from gradients of the macroscopic variables. Here, we consider the following estimates for this scale

$$\frac{1}{L_{\text{macro}}^{\theta}} = \theta, \quad (10)$$

$$\frac{1}{L_{\text{macro}}^{\varepsilon}} = \frac{1}{\varepsilon_0} \sqrt{\nabla_{\mu} \varepsilon_0 \nabla^{\mu} \varepsilon_0}, \quad (11)$$

$$\frac{1}{L_{\text{macro}}^{\sigma}} = \sqrt{\sigma_{\alpha\beta} \sigma^{\alpha\beta}}, \quad (12)$$

$$\frac{1}{L_{\text{macro}}^{\omega}} = \sqrt{\omega_{\alpha\beta} \omega^{\alpha\beta}}, \quad (13)$$

$$\frac{1}{L_{\text{macro}}^{\dot{u}}} = \sqrt{\dot{u}_{\alpha} \dot{u}^{\alpha}}. \quad (14)$$

That is, we only estimate the Knudsen number using different combinations of gradients of velocity or the local energy density. The corresponding Knudsen numbers are then given as $\text{Kn}_i = \tau_{\pi}/L_{\text{macro}}^i$. We note that in perfect fluid dynamics the scales (11) and (14) are algebraically related, but the same does not hold in viscous fluid dynamics where the difference depends also on the gradients of the shear-stress tensor. As a matter of fact, in viscous fluid dynamics $L_{\text{macro}}^{\dot{u}}$ and $L_{\text{macro}}^{\varepsilon}$ give rise to rather different macroscopic scales. For the sake of completeness we listed all the possible macroscopic scales that could be constructed from the gradients of velocity and of thermodynamic variables. However, in all the fluid-dynamical simulations performed for the purposes of this paper, the macroscopic scales $L_{\text{macro}}^{\theta}$ and $L_{\text{macro}}^{\varepsilon}$ were always considerably smaller than all the others. Therefore, in order to obtain the domain of applicability of fluid dynamics, it is enough to compare the microscopic scale only to $L_{\text{macro}}^{\theta}$ and $L_{\text{macro}}^{\varepsilon}$.

The range of Knudsen number values for which relativistic dissipative fluid dynamics remains valid has been estimated by comparing fluid-dynamical solutions to numerical solutions of the Boltzmann equation [30, 33, 37–42]. Such studies were performed considering dilute systems, for which the Boltzmann equation is able to provide a reasonable description. Nevertheless, they should

still be able to provide some understanding about the range of applicability of fluid dynamics in terms of the Knudsen number for other types of fluids. So far, the best information on these limits come from comparing the solutions of Israel-Stewart theory to numerical solutions of the Boltzmann equation in simplified situations, such as (1+1)-dimensional shock problem [39] or (0+1)-dimensional Bjorken expansion [37]. In these situations it was found that a $\text{Kn} < 0.5$ is required to get a good agreement between Israel-Stewart theory and the relativistic Boltzmann equation.

We note that the two tests mentioned above were done with Israel-Stewart theory, which is not the exact fluid-dynamical limit of the Boltzmann equation, see Refs. [31, 41]. Nevertheless, the fact that the two very different tests give the same limit for Kn , makes us confident that $\text{Kn} = 0.5$ provides a reasonable estimate for the limit of applicability of fluid dynamics. In this paper, we assume that this limit can be applied to the Knudsen number defined from the smallest macroscopic scale, that is,

$$\text{Kn} \equiv \frac{\tau_{\pi}}{L}, \quad L \equiv \min(L_{\text{macro}}^{\theta}, L_{\text{macro}}^{\varepsilon}). \quad (15)$$

Besides the perfect fluid limit $\text{Kn} \rightarrow 0$, another extreme behavior is the limit in which the microscopic scales become much longer than the macroscopic ones, i.e., $\text{Kn} \rightarrow \infty$. In this case the fluid breaks into free streaming particles. In practice one expects free streaming to become a good approximation to the evolution when viscosity becomes so large that $\text{Kn} \gtrsim 1$, see e.g. Ref. [38], for a demonstration of a transition from fluid like behavior to a free streaming behavior. In heavy ion collisions this transition is called decoupling or freeze-out, which usually is taken to happen at constant temperature, rather than determined from the condition $\text{Kn} \sim 1$, see however, Refs. [43–47] for a discussion on these kind of dynamical decoupling conditions.

Besides the Knudsen number, one can quantify the applicability of fluid dynamics using the inverse Reynolds number,

$$\text{R}_{\pi}^{-1} = \frac{\sqrt{\pi_{\mu\nu} \pi^{\mu\nu}}}{P_0}. \quad (16)$$

In the Navier-Stokes limit, where $\pi_{\mu\nu} \sim 2\eta\sigma^{\mu\nu}$, the inverse Reynolds number becomes proportional to the Knudsen number. However, in Israel-Stewart theory the shear-stress tensor satisfies a partial differential equation in which $2\eta\sigma^{\mu\nu}$ enters only as a source term. In this sense, the shear-stress tensor does not have to be equal to the Navier-Stokes value and the inverse Reynolds number corresponds to another measure to understand the applicability of fluid dynamics.

In the remainder of this paper, we shall verify how much the fluid-dynamical description can be driven out of its domain of applicability due to the large gradients present in a heavy ion collision. Of course, one should notice that it is basically not known how the breaking of the fluid-dynamical description will affect the different

heavy ion observables. Such a thing cannot be tested solely within a fluid-dynamical model. In this sense, the phenomenological implication of our findings will not be fully addressed in this work.

IV. FLUID DYNAMICAL MODEL FOR HEAVY-ION COLLISIONS

The main ingredients that affect the spacetime evolution and the values of the Knudsen numbers are the initial energy density profile, initialization time τ_0 and, obviously, the values of η/s . In order to better estimate the uncertainties in calculating the Knudsen numbers, we shall consider several different choices for these parameters.

Although we consider here a full (3+1)-dimensional expansion, the longitudinal expansion is treated analytically by assuming longitudinal boost-invariance. Within this approximation the longitudinal flow velocity is given by $v_z = z/t$, and the fluid dynamical quantities become independent of the spacetime rapidity $\eta_s = (1/2) \ln[(t+z)/(t-z)]$, i.e., they depend on the transverse coordinates, $\mathbf{x} = (x, y)$, and the longitudinal proper time, $\tau = \sqrt{t^2 - z^2}$, only. From a numerical point of view, this reduces the (3+1)-dimensional problem to a (2+1)-dimensional one. In this case it is also enough to give the initial conditions in the transverse plane only.

For the initial state in AA collisions we use two limits based on the optical Glauber model, eBC and eWN [48], where the energy density is proportional either to the density of binary collision (eBC),

$$\varepsilon_0(\mathbf{x}, \tau_0) = CT_A(\mathbf{x} - \mathbf{b}/2)T_A(\mathbf{x} + \mathbf{b}/2) \quad (17)$$

or to the density of wounded nucleons (eWN),

$$\begin{aligned} \varepsilon_0(\mathbf{x}, \tau_0) = & CT_A(\mathbf{x} - \frac{\mathbf{b}}{2}) \left[1 - \left(1 - \frac{\sigma_{NN} T_A(\mathbf{x} + \frac{\mathbf{b}}{2})}{A} \right)^A \right] \\ & + CT_A(\mathbf{x} + \frac{\mathbf{b}}{2}) \left[1 - \left(1 - \frac{\sigma_{NN} T_A(\mathbf{x} - \frac{\mathbf{b}}{2})}{A} \right)^A \right], \end{aligned} \quad (18)$$

where \mathbf{b} is the impact parameter, and $T_A(\mathbf{x})$ is the standard nuclear overlap function,

$$T_A(\mathbf{x}) = \int_{-\infty}^{\infty} dz \rho(\mathbf{x}, z), \quad (19)$$

where $\rho(\mathbf{x}, z)$ is the nucleon density parametrized as Wood-Saxon profile and σ_{NN} is the total inelastic nucleon-nucleon cross-section. In order to fully specify the initial conditions, we must also provide initial values to the fluid velocity u^μ and the shear-stress tensor $\pi^{\mu\nu}$. In this work these are always set initially to zero.

The initial state for pA collisions is taken to be

$$\varepsilon_0(\mathbf{x}, \tau_0) = CT_p(\mathbf{x})T_A(\mathbf{x}), \quad (20)$$

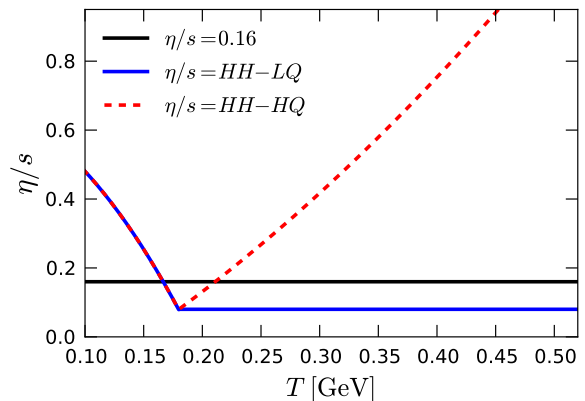


FIG. 1. (Color online) Different parametrizations of η/s .

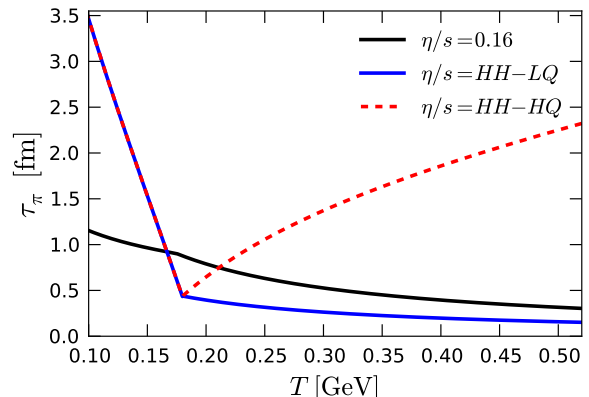


FIG. 2. (Color online) Relaxation times corresponding to the different η/s parametrizations.

where $T_p(\mathbf{x})$ is the nucleon overlap function, parametrized as Gaussian

$$T_p(\mathbf{x}) = \frac{1}{2\pi R^2} \exp[-\mathbf{x}^2/(2R^2)], \quad (21)$$

with parameter $R = 0.43$ fm, chosen to give the rms charge radius of the proton. Such initial profile should be good enough to estimate the Knudsen numbers reached in pA collisions.

The proportionality constants are fixed in such way that the multiplicity in the 0–5% most central AA collisions at RHIC and the LHC is reproduced. For the p+A collisions we consider several choices that give different final multiplicities. The initialization time is taken to be either $\tau_0 = 0.2$ fm or $\tau_0 = 1.0$ fm.

For the shear viscosity we use three different constant values, $\eta/s = 0.08, 0.16$ and 0.24 , and two temperature dependent parametrizations *HH-LQ* and *HH-HQ* from Refs. [12, 13]. These parametrizations of η/s are shown in Fig. 1, and the corresponding relaxation times in Fig. 2.

Finally, we have to specify an equation of state (EoS) that relates pressure and temperature to the local energy density. For this we use a lattice QCD based EoS from

Ref. [49], with a partial chemical freeze-out at $T_{\text{chem}} = 175$ MeV.

Once the initial conditions, EoS, and the transport coefficients are given, the equations of motion for shear-stress tensor, Eq. (4), and the conservation laws, Eq. (1), form a closed system of equations, that can be solved numerically. As a result, we obtain the spacetime evolution of all the quantities appearing in the energy-momentum tensor and, subsequently, we can calculate any of the macroscopic scales defined above. The numerical algorithm employed here to solve the equations of motion is introduced and discussed in Refs. [13, 50].

V. RESULTS

First, we consider the time evolution of semi-peripheral (20-30 %) Pb+Pb collisions at the LHC, with different parametrizations of $\eta/s(T)$, initialization times τ_0 and different initial states. Figures 3-8 show the time evolution of different quantities in the $(r = \sqrt{x^2 + y^2}, \tau)$ -plane along the $x = y$ diagonal. The impact parameter is always along the x -axis. We consider two different initialization times, $\tau_0 = 0.2$ fm and 1.0 fm.

In Fig. 3 we show the evolution of temperature with $\eta/s = 0.08$, $\tau_0 = 0.2$ fm and eBC initialization. Initially the temperature drops quickly due to the fast longitudinal expansion. In the later stages of the evolution the longitudinal expansion rate gradually decreases while, at the same time, the transverse velocity starts to build up, pushing the matter into the outward direction. This generates a characteristic shape for the constant temperature curves in the (r, τ) -plane. This figure also shows that a significant part of the evolution happens in the QCD transition region $T = 150$ -250 MeV, which is also the temperature region where the effects of shear viscosity on the evolution of the system is the strongest [13].

A. Spacetime evolution of the Knudsen numbers

Figure 4 shows the spacetime evolution of Kn_θ for the eBC initial state, with two different initialization times, $\tau_0 = 0.2$ fm (Left panels) and $\tau_0 = 1.0$ fm (Right panels), and three different η/s parametrizations, $\eta/s = 0.08$ (Top panels), $\eta/s = \text{HH-LQ}$ (Middle panels) and $\eta/s = \text{HH-LQ}$ (Bottom panels). Figure 5 shows the same cases, but for the eWN initialization. Figure 6 displays the spacetime evolution of Kn_ε for the same cases as in Fig. 4. The color coding in the figures divides the evolution roughly into three different regions:

- $\text{Kn} < 0.5$ where one expects fluid dynamical behavior (blue).
- $\text{Kn} = 0.5 \dots 1$ a transient region (green to yellow).
- $\text{Kn} > 1$ a free streaming region (red).

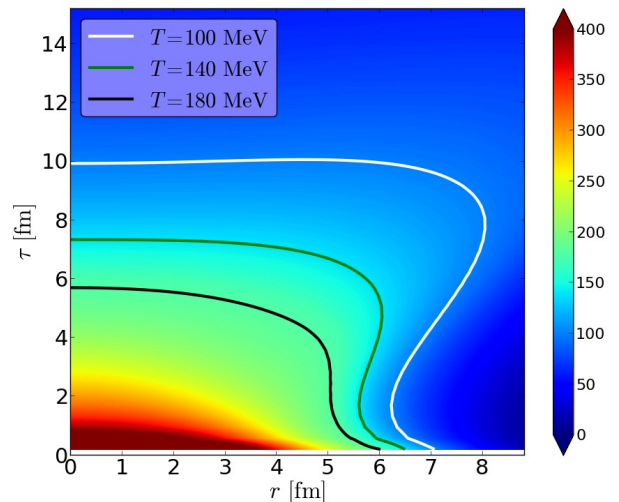


FIG. 3. (Color online) Spacetime evolution of temperature in 20 – 30 % centrality class in Pb+Pb collision at the LHC, with $\eta/s = 0.08$, $\tau_0 = 0.2$ fm and eBC initial state.

As already mentioned, it turns out that Kn_θ and Kn_ε from Eqs. (10) and (11) always give the smallest macroscopic scales and, therefore, are the most relevant when analyzing the applicability of fluid dynamics in heavy ion collisions. As can be seen from the figures, the expansion rate is the dominant scale in the early stages of the evolution, when the longitudinal expansion is very strong, while the energy density gradient is the dominant scale at the edge of the fireball.

While the different choices of initial times and initial conditions have a quantitative effect on the time evolution of both Knudsen numbers, their behavior is qualitatively the same for these choices. On the other hand, the same cannot be said about the shear viscosity coefficient. Even the qualitative behavior of the Knudsen numbers can change significantly as one varies this transport coefficient.

For the case of a constant $\eta/s = 0.08$, the Knudsen numbers are below the applicability limit $\text{Kn} \ll 0.5$ almost throughout all the spacetime evolution, with an exception at the edge of the fireball where the energy density gradients are very large. At small radius, there is no transition from a fluid-dynamical regime to a free-streaming regime, except at the very edge of the system. In other words, for the case of a constant η/s , the system never completely switches from a fluid regime to a particle regime. Therefore, when η/s is constant such transition is not physical, and must be implemented by hand. The common practice in simulations of heavy ion collisions is just to switch at a constant temperature hypersurface.

We note that the Knudsen numbers are basically linear with the shear viscosity coefficient. The larger the shear viscosity, the larger the Knudsen numbers become. For this reason when using the parametrizations HH-LQ or HH-HQ , which have the larger η/s values, except at the

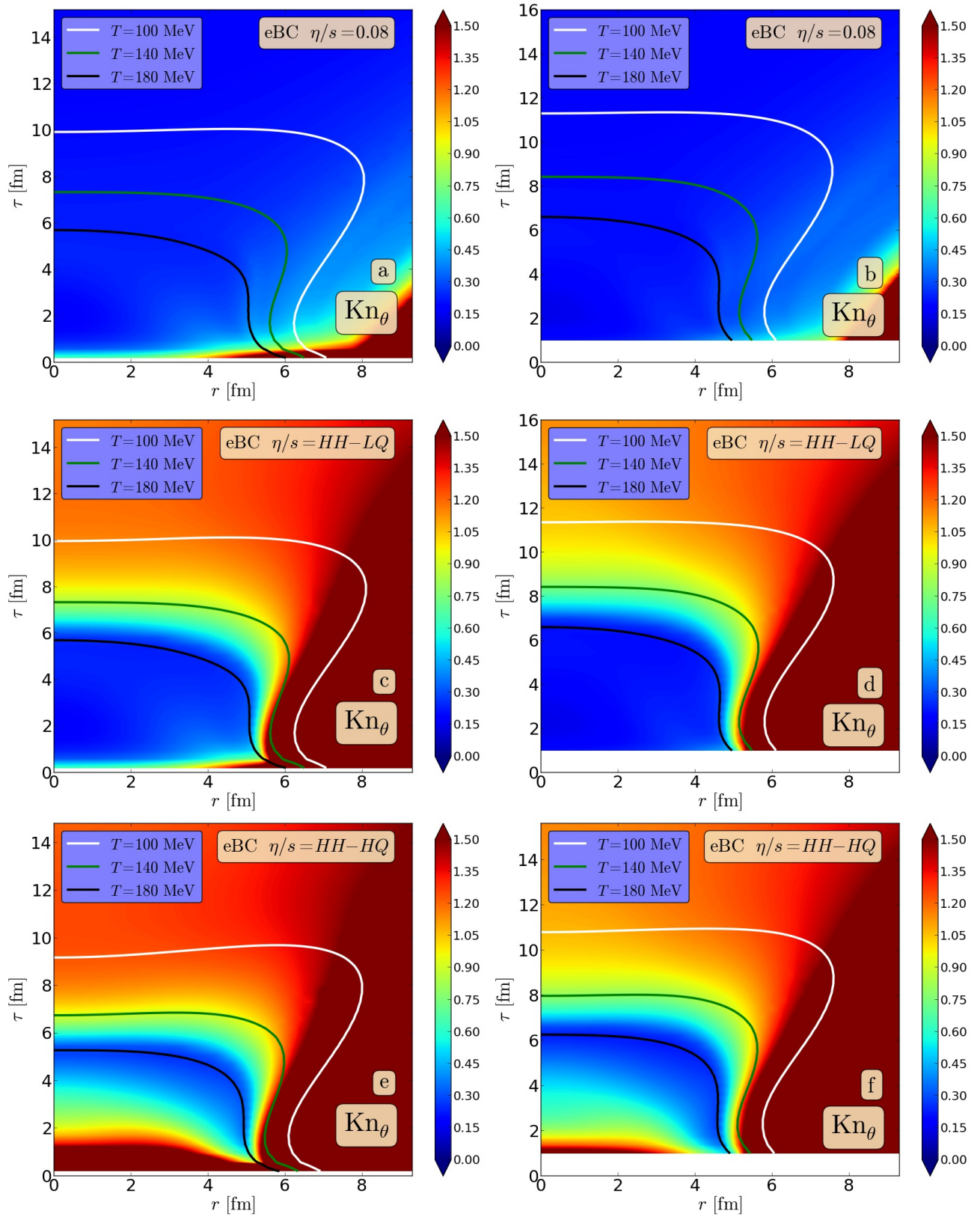


FIG. 4. (Color online) Spacetime evolution of Kn_θ in a Pb+Pb collision of the 20 – 30 % centrality class at the LHC, with eBC initial state. In the left panels [(a), (c) and (e)] the initial time is set to $\tau_0 = 0.2$ fm, while in the right panels [(b), (d) and (f)] $\tau_0 = 1.0$ fm. In the top [(a) and (b)], middle [(c) and (d)], and bottom [(e) and (f)] panels, the shear viscosity is set to $\eta/s = 0.08$, $\eta/s = HH-LQ$ and $\eta/s = HH-HQ$, respectively.

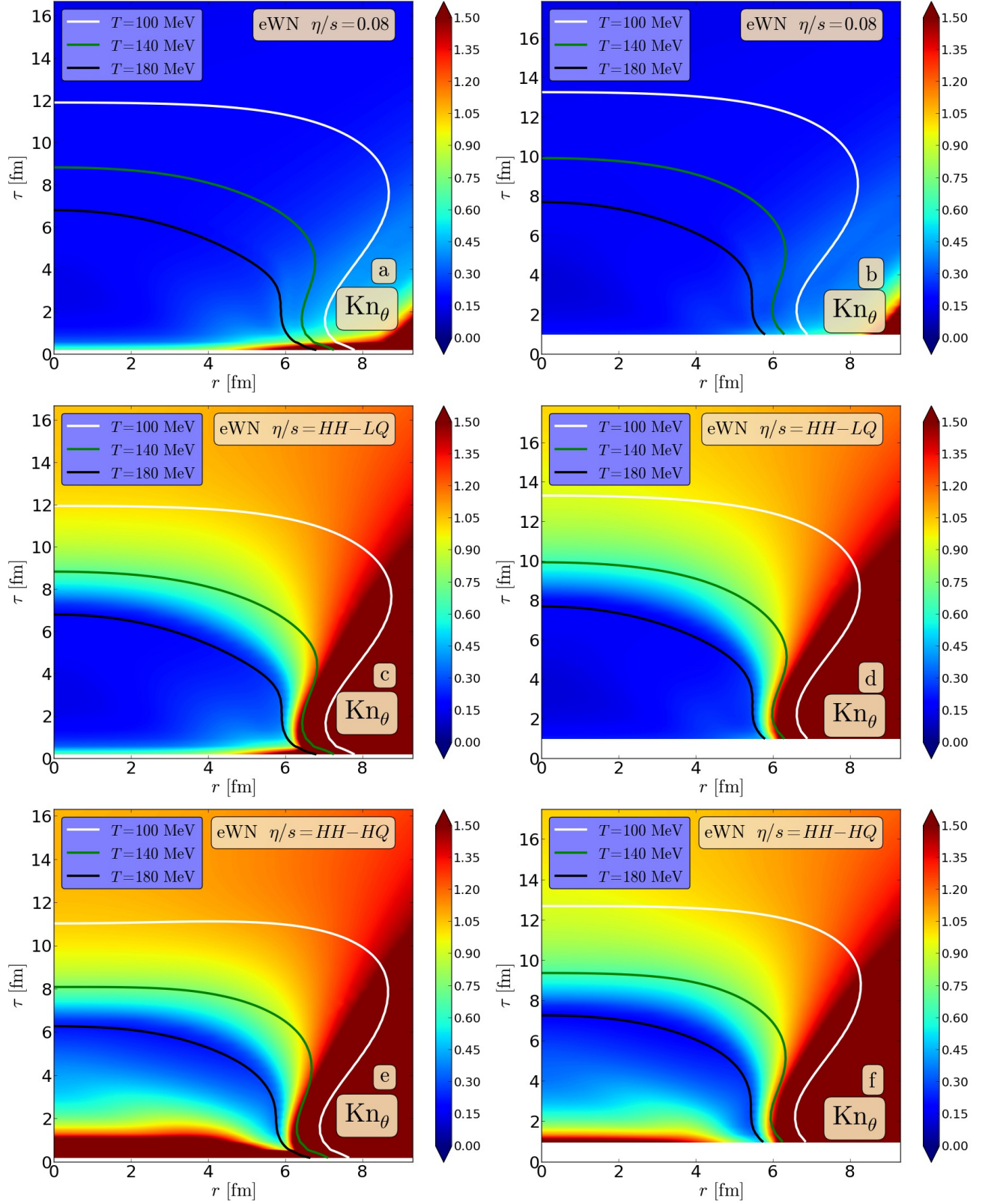


FIG. 5. (Color online) Spacetime evolution of Kn_θ in a Pb+Pb collision of the 20 – 30 % centrality class at the LHC, with eWN initial state. In the left panels [(a), (c) and (e)] the initial time is set to $\tau_0 = 0.2$ fm, while in the right panels [(b), (d) and (f)] $\tau_0 = 1.0$ fm. In the top [(a) and (b)], middle [(c) and (d)], and bottom [(e) and (f)] panels, the shear viscosity is set to $\eta/s = 0.08$, $\eta/s = \text{HH-LQ}$ and $\eta/s = \text{HH-HQ}$, respectively.

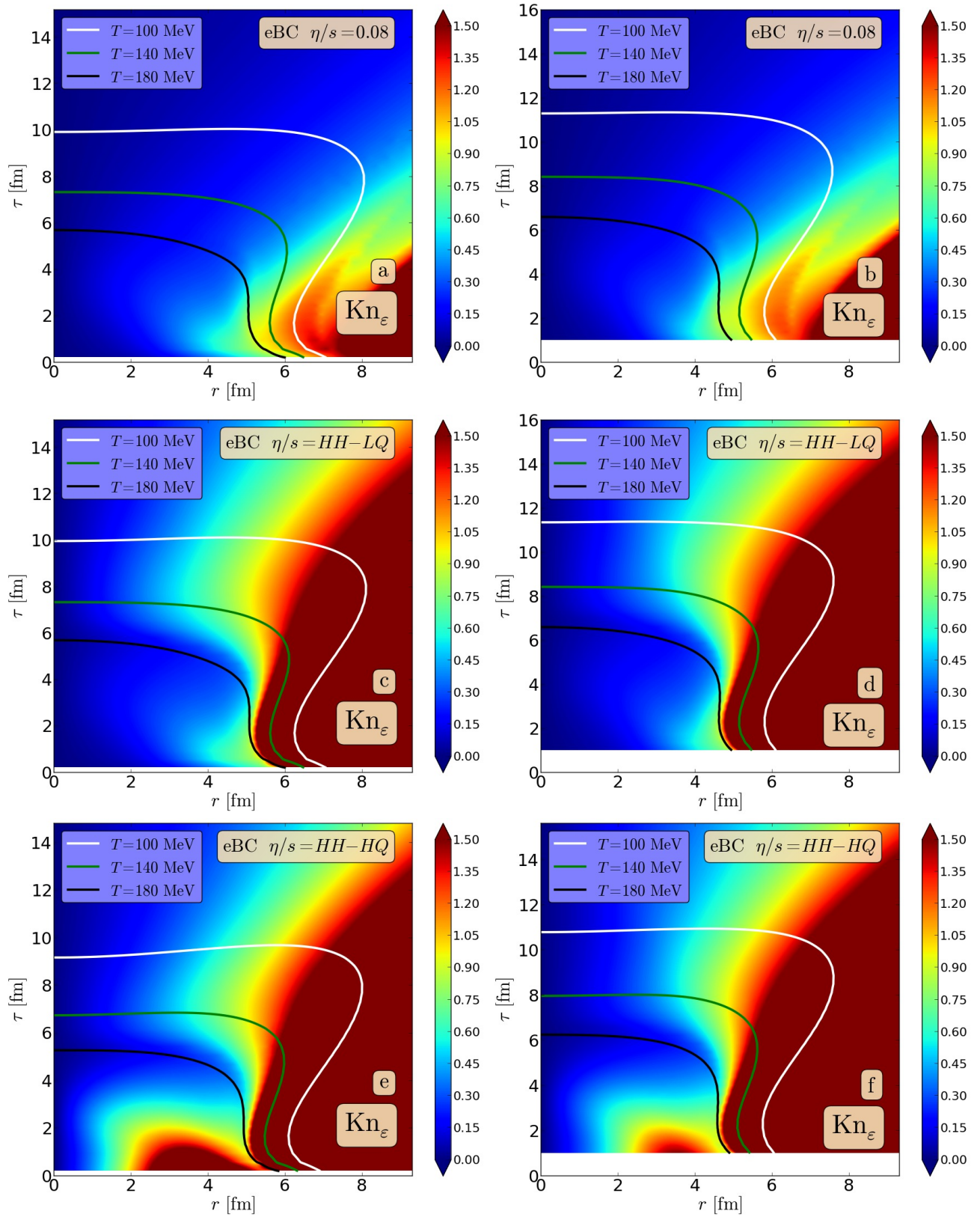


FIG. 6. (Color online) Spacetime evolution of Kn_ε in a Pb+Pb collision of the 20 – 30 % centrality class at the LHC, with eBC initial state. In the left panels [(a), (c) and (e)] the initial time is set to $\tau_0 = 0.2$ fm, while in the right panels [(b), (d) and (f)] $\tau_0 = 1.0$ fm. In the top [(a) and (b)], middle [(c) and (d)], and bottom [(e) and (f)] panels, the shear viscosity is set to $\eta/s = 0.08$, $\eta/s = HH-LQ$ and $\eta/s = HH-HQ$, respectively.

minimum, we observe a drastic increase of the Knudsen numbers.

If we use a realistic hadronic η/s , which increases as the temperature decreases, it is possible to observe a transition from a fluid-dynamical behavior ($\text{Kn} < 0.5$) to a free-streaming behavior ($\text{Kn} > 1$). Naturally, the $\text{Kn} = 1$ hypersurfaces are never equal to the constant temperature hypersurfaces. Nevertheless, it is not impossible to find a case in which temperature stays approximately constant along the $\text{Kn} = 1$ hypersurface. For example in Fig. 4e the $T = 140$ MeV hypersurface is very close to the $\text{Kn}_\theta = 1$ hypersurface. So far, we have not found any example where this happens for a $\text{Kn}_\varepsilon = 1$ hypersurface.

When using the *HH-LQ* parametrization, which has a constant $\eta/s = 0.08$ in the high temperature phase, the Knudsen numbers are still clearly below 0.5 in the high-temperature phase ($T > 180$ MeV), except in the very early stages of the evolution. If we use instead the *HH-HQ* parametrization with a strongly increasing η/s in the high-temperature phase, there is only a rather small region around the minimum η/s where fluid dynamics is clearly valid.

In Fig. 7 we show the time evolution of the Knudsen numbers in pA collisions using the *HH-LQ* parametrization of η/s . The initial energy density profile is normalized in such a way that the final charged particle multiplicity is $dN_{ch}/d\eta = 270$. In this case the lifetime and size of system is considerably smaller than those achieved in AA collisions. Also, the Knudsen number reached during the evolution grow considerably faster than in AA collisions: Knudsen number values at the $T = 180$ MeV hypersurface are already large enough to exceed the $\text{Kn} = 0.5$ limit. As a matter of fact, At the $T = 100$ MeV hypersurface the fluid dynamical description is clearly out of its applicability domain, with all Kn_θ values above 1.5. One can see that in pA collisions the fluid-dynamical description is pushed to its extreme, even with a constant $\eta/s = 0.08$ in the QGP phase. If a temperature dependent η/s were used also in the QGP phase, the situation would be even more extreme and fluid dynamics would be out of its domain of applicability even in the early stages of the evolution. We note that, even though the values of Knudsen numbers are quantitatively different in pA and AA collisions, the qualitative behavior of the Knudsen number as a function of spacetime is rather similar in both cases.

So far we have not shown any results involving the inverse Reynolds number. This is because, the range values of inverse Reynolds number that quantifies the applicability of the fluid-dynamical description is not very well known. Commonly, it is accepted is that R_π^{-1} should be smaller than 1, but such limit was never extracted from systematically comparing solutions of fluid dynamics and Boltzmann equation. We note that the applicability of the freeze-out formalism currently employed in simulations of heavy ion collisions depends on the inverse Reynolds numbers, since the non-equilibrium single particle momentum distribution grows linearly with the

inverse Reynolds number, i.e.

$$\delta f(k) \sim \frac{\pi^{\mu\nu}}{\varepsilon_0 + p_0} k_\mu k_\nu, \quad (22)$$

where k^μ is the 4-momenta of the particle being emitted. In Fig. 8 we show the time evolution of the inverse Reynolds number for the same case as in Fig. 4e. As one can read off from the plot, the values of inverse Reynolds number become larger than 1 at the edge of the system. From a practical point of view it is difficult to find a constant temperature hypersurface where the inverse Reynolds number is always below 1. Note that even by choosing a constant Knudsen number hypersurface it is not guaranteed that the values of the inverse Reynolds number would always be less than 1. As mentioned in Sec. III, this happens because in transient fluid dynamics the Knudsen number is not proportional to the inverse Reynolds number, i.e., their relation is dynamical rather than algebraic.

We note that in Ref. [51] it was observed that the inverse Reynolds number is large during a significant fraction of the lifetime of the system formed in p+Pb collisions.

B. Maximum effective η/s

In this subsection we investigate the systematics of the applicability of the fluid dynamical description in more detail. We estimate the average values of η/s where the fluid dynamical description breaks down, and how those values depend on the centrality of the collisions, the initial conditions and the initialization time. Moreover, we also check what are the allowed η/s values for fluid dynamics to work also in the pA collisions.

For this purpose we first construct an estimate for the maximum η/s in each spacetime point, and then proceed to define a maximum effective η/s , for a given initial state and collision centrality, by taking an average of the local maximum η/s over the whole spacetime evolution.

Here we have calculated the Knudsen numbers as

$$\text{Kn}_i = \frac{\tau_\pi}{L_i} = \frac{5\eta}{\varepsilon_0 + p_0} \frac{1}{L_i}, \quad (23)$$

where L_i is one of the macroscopic scales defined above. If the macroscopic gradients depend sufficiently weakly on the values of η/s , as it turns out to be the case, we can calculate L_i with any parametrization of η/s in the actual fluid dynamical calculation. This allows us then to invert the above equation and calculate what is the value of η/s that gives a Knudsen number that is at the limit of the applicability of fluid dynamics, i.e. $\text{Kn} = \text{Kn}_{\text{max}}$. In each spacetime point, this will give a maximum allowed η/s for fluid dynamics to remain valid,

$$\eta/s|_{\text{max}} = \text{Kn}_{\text{max}} \frac{(\varepsilon_0 + p_0)L_i}{5s}. \quad (24)$$

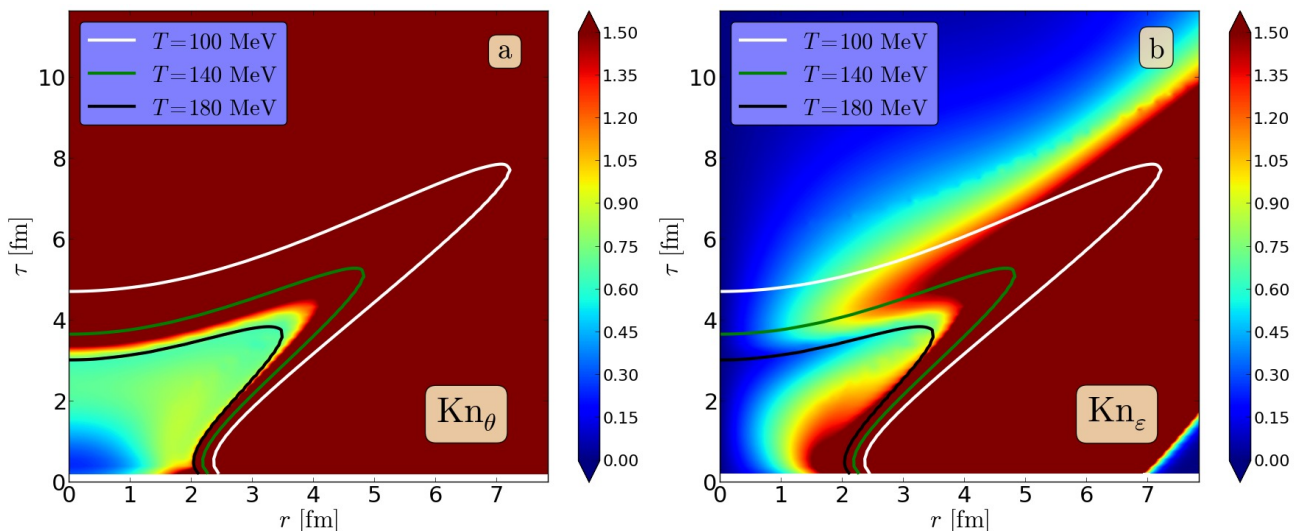


FIG. 7. (Color online) Spacetime evolution of the Knudsen numbers in p+Pb collision at the LHC, with $\eta/s = HH-LQ$ and $dN_{ch}/d\eta = 270$. (a) Kn_θ and (b) Kn_ϵ .

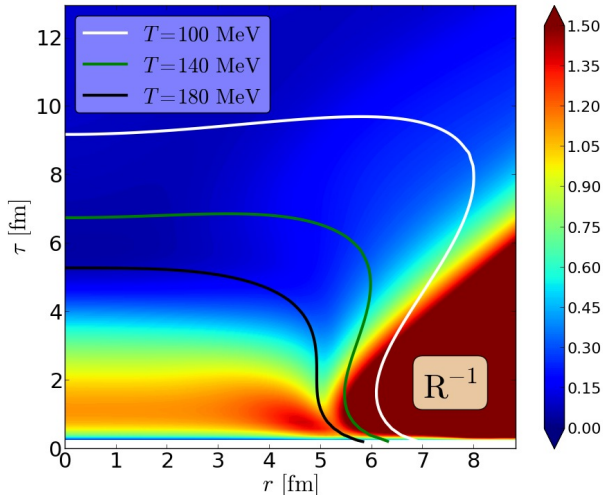


FIG. 8. (Color online) Spacetime evolution of the Reynolds number in 20 – 30 % centrality class in Pb+Pb collision at the LHC, with $\eta/s = HH-HQ$ and eBC initial state.

Here we take the macroscopic scale to be $L_i = \min(L_\theta, L_\epsilon)$. For each collision system, we then calculate a maximum effective η/s by taking an entropy weighted average over the whole spacetime evolution,

$$\left\langle \frac{\eta}{s} \right\rangle_{\max} = \frac{\int_{T>T_f} d\tau dx dy \tau s(\eta/s|_{\max})}{\int_{T>T_f} d\tau dx dy \tau s}, \quad (25)$$

where $T_f = 100$ MeV. The results are not very sensitive to the choice of T_f , e.g. $T_f = 180$ MeV would change the η/s limit by order of 10 % at most.

In principle, the r.h.s. of Eq. (24) depends also on the actual values of η/s in the fluid dynamical calculation. However, we have tested that this dependence is

weak. We further note that if a fluid-dynamical calculation is done with a constant η/s , with a value given by Eq. (25), the resulting spacetime averaged Knudsen number is approximately $Kn \sim Kn_{\max}$. In this sense the limit $\langle \eta/s \rangle_{\max}$ can be considered as a maximum effective η/s . As discussed in Sec. III, we use here $Kn_{\max} = 0.5$.

Figure 9 shows the maximum allowed η/s for Pb+Pb collisions at the LHC as a function of centrality. The different curves correspond to different choices of the initial conditions and τ_0 . The thickness of the curves indicates the uncertainty of the estimate due to the actual values of the η/s in the fluid dynamical calculation of the r.h.s. of Eq. (24). We have varied constant η/s between 0.08 and 0.24 and also used the two temperature dependent parametrizations $HH-LQ$ and $HH-HQ$. The smaller Figure inside, where the lower (upper) set of points are for $\tau_0 = 0.2$ (1.0) fm, show the same estimate for pPb collisions as a function of charged hadron multiplicity.

As can be read off from the figure, the limit for the shear viscosity is of the order $\eta/s \sim 0.1 - 0.2$. These values are similar in magnitude to the estimates for the QGP shear viscosity. As expected, increasing τ_0 or changing initial conditions from eBC to eWN create more favorable conditions for fluid dynamics to be applicable. Both of these changes have similar effect on the η/s limit.

The collision geometry in AA collisions at RHIC and at LHC is rather similar and the difference in η/s limit between RHIC and LHC is of the same order as the uncertainty estimate in Fig. 9. On the other hand, a much smaller system formed in pPb collisions results in drastically smaller values for η/s limit, questioning at least quantitatively how well fluid dynamics can describe such small systems.

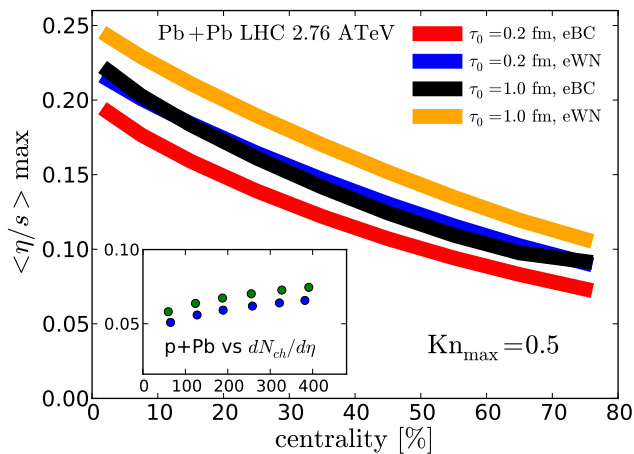


FIG. 9. (Color online) The dependence of the $\langle \frac{\eta}{s} \rangle_{\max}$ on the initial state, initialization time in Pb+Pb collisions at the LHC. The uncertainty band is obtained by varying η/s parametrization, see text. The small figure inside shows the same estimate for pPb collisions with different multiplicities. The lower (upper) set of points show the estimate with $\tau_0 = 0.2$ (1.0).

VI. CONCLUSIONS

We have calculated the values of different Knudsen numbers in ultrarelativistic heavy-ion collisions as well as in pPb collisions and, based on these values, we have estimated the maximum allowed η/s values for which the fluid dynamical description of the spacetime evolution of the collisions is still valid.

We found that two macroscopic scales, the expansion rate and the energy density gradient, always give the tightest limits for the applicability of fluid dynamics. The expansion rate is the dominant macroscopic scale during the early stages of the evolution and near the center of the system, while the energy density gradients are large near the edge of the system. Other estimates of the macroscopic scales give typically Knudsen numbers much smaller than these two choices.

Obviously, the exact values of the Knudsen numbers depend strongly on the chosen η/s parametrization. For example in AA collisions with a constant $\eta/s = 0.08$ the whole evolution is always below the applicability limit $Kn = 0.5$, but leads to a rather strange picture where the system never fully decouples to a free-streaming particles. On the other hand, the temperature dependent parametrizations considered here give a decoupling re-

gion with a similar shape as constant temperature contours. It then depends on the high-temperature behavior of η/s , whether almost all the QGP evolution is describable with fluid dynamics, or just a small region around the QCD transition. In pPb collisions the situation is considerably more difficult: Knudsen numbers are above the applicability limit almost during the whole evolution even with a small constant $\eta/s = 0.08$ in the QGP phase.

Based on the calculated values of the Knudsen numbers, we further estimated the maximum allowed η/s for the fluid dynamical description to be valid for the heavy-ion collisions. The uncertainties in these estimates were determined by varying the initial conditions, initialization time and the η/s parametrizations in the actual fluid dynamic calculation. In AA collisions we found that these estimates give η/s limits that are of the same order than the typical values of $\eta/s = 0.1 \dots 0.2$ found from the comparisons between the RHIC and LHC data with the predictions of fluid dynamical models for AA collisions [3–14]. The limits depend on the centrality of the collision, dropping by approximately a factor of two from central (0-5 %) to peripheral (70-80 %) collisions. The difference between RHIC and LHC is small.

Although, these estimates indicate that fluid dynamics is applicable in heavy ion collisions, perhaps even at quantitative level, we are still very close to the applicability limit and there can still be large corrections to spacetime evolution even in central collisions. Furthermore, we cannot reliably study simulations with larger values of η/s without using a description that goes beyond usual fluid dynamics.

The situation for pA collisions is even more difficult, as the η/s limit is already clearly below $\eta/s \sim 0.1$ and depends only weakly on the charged particle multiplicity. As one expects that a same type of matter is created both in AA and pA collisions, the transport properties of the matter should also be the same. This makes it hard to trust quantitatively the predictions of fluid dynamics in pA collisions. We have not considered event-by-event fluctuations of the initial densities here, but we note that including those could bring the local conditions in AA collisions closer to the conditions in pA collisions.

VII. ACKNOWLEDGMENTS

We thank P. Huovinen and D. H. Rischke for comments and discussions. The work of H. Niemi was supported by Academy of Finland, Project No. 133005. G. S. Denicol is supported by a Banting Fellowship of the Natural Sciences and Engineering Research Council of Canada.

[1] U. W. Heinz and R. Snellings, Annu. Rev. Nucl. Part. Sci. **63**, 123 (2013).
 [2] P. Huovinen, Int. J. Mod. Phys. E **22**, 1330029 (2013).

[3] P. Romatschke and U. Romatschke, Phys. Rev. Lett. **99**, 172301 (2007).
 [4] M. Luzum and P. Romatschke, Phys. Rev. C **78**, 034915 (2008) [Erratum-ibid. C **79**, 039903 (2009)].

- [5] B. Schenke, S. Jeon and C. Gale, Phys. Rev. Lett. **106**, 042301 (2011); Phys. Rev. C **85**, 024901 (2012); Phys. Lett. B **702**, 59 (2011).
- [6] C. Gale, S. Jeon, B. Schenke, P. Tribedy and R. Venugopalan, Phys. Rev. Lett. **110**, 012302 (2013).
- [7] H. Song, S. A. Bass, U. Heinz, T. Hirano and C. Shen, Phys. Rev. Lett. **106**, 192301 (2011) [Erratum-ibid. **109**, 139904 (2012)]; Phys. Rev. C **83**, 054910 (2011) [Erratum-ibid. C **86**, 059903 (2012)].
- [8] H. Song, S. A. Bass and U. Heinz, Phys. Rev. C **83**, 054912 (2011) [Erratum-ibid. C **87**, 019902 (2013)].
- [9] C. Shen, U. Heinz, P. Huovinen and H. Song, Phys. Rev. C **82**, 054904 (2010); Phys. Rev. C **84**, 044903 (2011).
- [10] P. Bozek, Phys. Rev. C **81**, 034909 (2010); Phys. Rev. C **85**, 034901 (2012).
- [11] P. Bozek and I. Wyskiel-Piekarska, Phys. Rev. C **85**, 064915 (2012).
- [12] H. Niemi, G. S. Denicol, P. Huovinen, E. Molnar, and D. H. Rischke, Phys. Rev. Lett. **106**, 212302 (2011).
- [13] H. Niemi, G. S. Denicol, P. Huovinen, E. Molnar, and D. H. Rischke, Phys. Rev. C **86**, 014909 (2012).
- [14] R. Paatelainen, K. J. Eskola, H. Niemi and K. Tuominen, Phys. Lett. B **731**, 126 (2014).
- [15] C. E. Aguiar, Y. Hama, T. Kodama and T. Osada, Nucl. Phys. A **698**, 639 (2002); O. Socolowski, Jr., F. Grassi, Y. Hama and T. Kodama, Phys. Rev. Lett. **93**, 182301 (2004); R. Andrade, F. Grassi, Y. Hama, T. Kodama and O. Socolowski, Jr., Phys. Rev. Lett. **97**, 202302 (2006); J. Takahashi, B. M. Tavares, W. L. Qian, R. Andrade, F. Grassi, Y. Hama, T. Kodama and N. Xu, Phys. Rev. Lett. **103**, 242301 (2009).
- [16] B. Alver and G. Roland, Phys. Rev. C **81**, 054905 (2010) [Erratum-ibid. C **82**, 039903 (2010)].
- [17] A. Dumitru and Y. Nara, Phys. Rev. C **85**, 034907 (2012).
- [18] B. Schenke, P. Tribedy and R. Venugopalan, Phys. Rev. Lett. **108**, 252301 (2012).
- [19] G. -Y. Qin and B. Mller, Phys. Rev. C **89**, 044902 (2014).
- [20] K. Werner, M. Bleicher, B. Guiot, Iu. Karpenko and T. Pierog, arXiv:1307.4379.
- [21] P. Bozek and W. Broniowski, arXiv:1401.2367 [nucl-th].
- [22] L.D. Landau and E.M. Lifshitz, *Fluid Mechanics*, (Pergamon; Addison-Wesley, London, U.K.; Reading, U.S.A., 1959).
- [23] S. Chapman and T.G. Cowling, *The mathematical theory of non-uniform gases*, 3rd edition (Cambridge University Press, Cambridge, 1970).
- [24] D. Burnett, Proc. Lond. Math. Soc. **39**, 385 (1935); Proc. Lond. Math. Soc. **40**, 382 (1936).
- [25] W.A. Hiscock and L. Lindblom, Ann. Phys. (N.Y.) **151**, 466 (1983); Phys. Rev. D **31**, 725 (1985); Phys. Rev. D **35**, 3723 (1987); Phys. Lett. A **131**, 509 (1988); Phys. Lett. A **131**, 509 (1988).
- [26] G. S. Denicol, T. Kodama, T. Koide and P. Mota, J. Phys. G **35**, 115102 (2008).
- [27] S. Pu, T. Koide and D. H. Rischke, Phys. Rev. D **81**, 114039 (2010).
- [28] W. Israel and J. M. Stewart, Ann. Phys. (N.Y.) **118**, 341 (1979).
- [29] H. Grad, Comm. Pure Appl. Math. **2**, 331 (1949).
- [30] G. S. Denicol, T. Koide and D. H. Rischke, Phys. Rev. Lett. **105**, 162501 (2010).
- [31] G. S. Denicol, H. Niemi, E. Molnar and D. H. Rischke, Phys. Rev. D **85**, 114047 (2012).
- [32] G. S. Denicol, E. Molnar, H. Niemi and D. H. Rischke, Eur. Phys. J. A, **48** **11**, 170 (2012).
- [33] E. Molnár, H. Niemi, G. S. Denicol and D. H. Rischke, arXiv:1308.0785 [nucl-th].
- [34] B. Betz, D. Henkel and D. H. Rischke, Prog. Part. Nucl. Phys. **62**, 556 (2009).
- [35] B. Betz, G. S. Denicol, T. Koide, E. Molnar, H. Niemi and D. H. Rischke, EPJ Web Conf. **13**, 07005 (2011).
- [36] G. S. Denicol, J. Noronha, H. Niemi and D. H. Rischke, Phys. Rev. D **83**, 074019 (2011); G. S. Denicol, J. Noronha, H. Niemi and D. H. Rischke, J. Phys. G **38**, 124177 (2011).
- [37] P. Huovinen and D. Molnar, Phys. Rev. C **79**, 014906 (2009).
- [38] I. Bouras, E. Molnar, H. Niemi, Z. Xu, A. El, O. Fochler, C. Greiner and D. H. Rischke, Phys. Rev. Lett. **103**, 032301 (2009).
- [39] I. Bouras, E. Molnar, H. Niemi, Z. Xu, A. El, O. Fochler, C. Greiner and D. H. Rischke, Phys. Rev. C **82**, 024910 (2010).
- [40] D. Molnar and P. Huovinen, Phys. Rev. Lett. **94**, 012302 (2005).
- [41] G. S. Denicol, H. Niemi, I. Bouras, E. Molnar, Z. Xu, D. H. Rischke and C. Greiner, arXiv:1207.6811 [nucl-th].
- [42] R. Yano and K. Suzuki, Phys. Rev. D **86**, 083522 (2012).
- [43] A. Dumitru, Phys. Lett. B **463** 138 (1999).
- [44] C. M. Hung and E. V. Shuryak, Phys. Rev. C **57** 1891 (1998).
- [45] U. W. Heinz and G. Kestin, Eur. Phys. J. ST **155**, 75 (2008).
- [46] K. J. Eskola, H. Niemi and P. V. Ruuskanen, Phys. Rev. C **77**, 044907 (2008).
- [47] H. Holopainen and P. Huovinen, J. Phys. Conf. Ser. **389**, 012018 (2012).
- [48] P. F. Kolb, U. W. Heinz, P. Huovinen, K. J. Eskola and K. Tuominen, Nucl. Phys. A **696**, 197 (2001).
- [49] P. Huovinen and P. Petreczky, Nucl. Phys. A **837**, 26 (2010).
- [50] E. Molnar, H. Niemi and D. H. Rischke, Eur. Phys. J. C **65**, 615 (2010).
- [51] A. Bzdak, B. Schenke, P. Tribedy and R. Venugopalan, Phys. Rev. C **87**, no. 6, 064906 (2013).